Computer Physics Communications 236 (2019) 86–94

Contents lists available at ScienceDirect

Computer Physics Communications

journal homepage: www.elsevier.com/locate/cpc

Optimal determination of force field parameters for reduced molecular dynamics model

Hyun-Seok Kim [a], Jae-Hyun Kim [b], Song-Hyun Cha [b], Seonho Cho [b,*]

[a] Korea Research Institute of Ships and Ocean Engineering (KRISO), 1312-31 Yuseong-daero, Yuseong-gu, Daejeon 34103, Republic of Korea
[b] Department of Naval Architecture and Ocean Engineering, Seoul National University, 1 Gwanak-ro, Gwanak-gu, Seoul 08826, Republic of Korea

ARTICLE INFO

Article history:
Received 26 August 2017
Received in revised form 2 October 2018
Accepted 23 October 2018
Available online 15 November 2018

Keywords:
Gradient-based optimization
Adjoint design sensitivity
Molecular dynamics
NVT ensemble
Gold nanoparticle
Mica substrate

ABSTRACT

Using a gradient-based optimization method, the time-consuming atomistic model of substrate is replaced by computationally efficient Lennard-Jones (L-J) potential walls whose parameters are determined to appropriately represent the interactions between the nanoparticles and the substrate. To obtain the required design sensitivity with respect to design variables for the constant temperature molecular dynamics (MD) simulations that use the Nosé–Hoover thermostat, the finite difference method is impractical due to the huge amount of computational costs. Thus, we developed an adjoint design sensitivity analysis (DSA) method that is efficient for the system of many design variables. In numerical examples, we replace the complicated and time-consuming silicate structure to a multiple layer model of L-J potential wall, through the design optimization that includes the design variables of ϵ, σ, and the positions of each layer. The objective is to minimize the squared difference of time averaged performance between the full and the reduced models during the whole time span. The proposed method could lead to a significant reduction of computational costs, together with comparable outcomes from MD simulations.

1. Introduction

Nowadays, interest in molecular dynamics (MD) simulations has rapidly increased due to the demand of nanoscale manufacturing and applications. To overcome the limitation of the conventional continuum-based macroscale approach and to understand and elucidate nanoscale phenomena, the MD-based simulations have become one of the promising choices by researchers in various fields. Furthermore, the increased computational performance and enhanced parallel computing enable the MD simulations to be widely utilized in both academic and industrial environments to study various mechanical, chemical, and biological nanoscale systems. Nevertheless, when it comes to the design optimization of nanoscale materials, which are so far not fully developed yet but could be essential for future research, hundreds of MD simulations are required so that the reduction of computing costs in a simulation is crucial. The objective of this paper is to determine parameters in Lennard-Jones (L-J) potential walls to appropriately represent the interactions between nanoparticles and substrate, using a gradient-based optimization method to replace the time-consuming model of bulk substrates by the potential walls.

Even though real experiments have revealed many of new concepts and various phenomena in nanoscale, it is extremely difficult and also limited to investigate the microscopic, dynamical, and thermodynamic properties of systems through real experimental approaches. The MD simulations provide a suitable framework for exploring and elucidating the physically complex phenomena at an atomistic level. To obtain meaningful results from the MD simulations, one of the major concerns is to select the appropriate interatomic potentials that precisely represent the behavior of atoms. The interatomic potentials include the parameters which are determined by a variety of methods depending on the atom types involved. The estimation of the potential parameters has been attempted by a number of researchers [1,2] according to the theoretical basis of equations; the attractive dispersion force by the Slater–Kirkwood equation [3] and the repulsive term from van der Waals radii of atoms [4]. Then, the parameters are adjusted by the crystal packing [5] and other experimental data. One of the simple experimental results available to test the validity of the potential parameters may be the second virial coefficient of a gas composed of atoms in question, since the virial coefficient can be calculated from the interaction between constituent atoms. The interatomic potentials usually involve complicated terms and thus require additional treatments. If bulky substrates, aqueous solutions, or large bio-structures are involved in the MD simulations, we should include the pairwise force, many body forces, additional bonding, angle, and dihedral terms need to be included, which results in one of the major drawbacks from a computational point of view. For the interactions of heterogeneous materials in most of cases, the interatomic potential is generally simplified to

* Corresponding author.
E-mail address: secho@snu.ac.kr (S. Cho).

https://doi.org/10.1016/j.cpc.2018.10.019
0010-4655/

a pairwise Lennard Jones (L-J) potential form by combining the pairwise terms of each material through Lorentz–Berthelot mixing rules. Nevertheless, the computational costs are still prohibitively expensive even though the massively parallel computing scheme is employed. This implies that the significant portion of computation costs is squandered for simulating the bulk substrates which is not the major concern of the MD simulations. The objective of this paper is to determine parameters in Lennard-Jones (L-J) potential walls to appropriately represent the interactions between nanoparticles and substrate, using a gradient-based optimization method to replace the time-consuming model of bulk substrates by the potential walls.

To reduce the degrees of freedom (DOF) of full atomistic models, coarse-grained (CG) models that combine multiple atoms into one group (a CG bead) are developed. One of the challenges in the CG models is to develop a rigorous atomistic to CG methodology that allows, as accurately as possible, the estimation of the CG effective interactions. There are several CG methods used to derive the CG effective forces (or potentials): (i) MARTINI force field which fits thermodynamic properties such as free energy in the system [6], (ii) Reverse Monte-Carlo method [7], and Iterative Boltzmann Inversion [8] which minimizes the differences between the calculated and the reference averages of structural properties like a radial distribution function or a structure factor, and (iii) force matching approaches [9], where the instantaneous CG forces are fitted to the forces from full MD simulations. The choice of CG method depends on the nature of the system we are dealing with. The task of this paper is to closely observe the movement of the nanoparticles on the substrate. The atomistic motion for a nanoparticle is expressed as fully as possible, and for a substrate with little motion, it is expressed as a reduced model. For this purpose, we proposed a new method instead of the using the existing CG method to replace the substrate with the virtual L-J potential walls. The parameters of the virtual LJ potential walls are fitted to minimize the potential energy difference with the full model using a design sensitivity analysis (DSA) method. A simulation using the virtual L-J potential wall model confirmed a significant reduction of computational costs.

Design sensitivity analysis (DSA) aims at describing how much output values are affected by the changes in input values. Mathematically, the DSA methods have well developed based on continuum mechanics for structural systems [10]. Until now, most of researches on the DSA have been devoted to static mechanical problems. Recently, efficient and accurate DSA methods for transient dynamic problems are attracting researchers' attention in various disciplines. Since the MD is one of the transient dynamic problems, the DSA for transient dynamic problems is indispensable for the design of nanoscale problems. Dynamic problems require the time integration of partial differential equations to compute dynamics responses. For transient dynamic problems with large deformation elastic–plastic materials, an analytical DSA method [11,12] is developed in the updated Lagrangian formulation using a direct differentiation method (DDM). The adjoint variable method (AVM) for transient dynamics was well established in the reference [10] and the corresponding adjoint system turned out to be a terminal value problem. Hsieh and Arora [13] developed DSA methods using both the DDM and AVM for dynamic problems with point-wise constraints. Tsay and Arora [14] derived nonlinear DSA for path-dependent problems using total Lagrangian formulation considering geometrical and material nonlinearities. However, they follow all the history of solution procedure for the DSA because the dynamic equations for both original responses and design sensitivities are path-dependent. This makes it difficult to extend the DSA methods to MD simulations since the adjoint system that corresponds to the MD simulations is usually a path-dependent problem.

The MD is a typical transient dynamic problem but a few literature is available for the DSA methods of transient dynamics. Extension of DSA methods to the atomic level transient dynamics was never attempted due to the limitation of computational resources and the lack of efficient DSA method even though the MD simulations were already established. When the performance measure is only dependent on the state at terminal time and the internal force term is linear with respect to the displacement due to the harmonic approximation of the inter-atomic potential, the adjoint equation of motion can be independently solved from the original system. In that case, there is an advantage of saving the computational storage to keep the original response history [15,16]. In the case of non-linear internal forces, however, the adjoint equations depend on the path of original responses and thus the tangent stiffness in the adjoint systems changes with time. In this case, the adjoint problem is time history dependent, which means that we must follow all the history of response analysis to solve the problem.

The DSA [17] in the MD simulations can be utilized in various fields. For instance, instead of using the expensive first-principle quantum-mechanical (QM) method, the sensitivities of atomic mass m and the L-J parameter σ and ϵ can be utilized to develop an empirical interatomic potential [18]. The DSA method in this paper is developed in a general manner and can be easily extended to other general types of performance measures like the kinematics of atoms, the temperature of system, and so on. Even though the interatomic potential to precisely describe the atomic behaviors is constructed, the significant amount of computing costs is still squandered to compute the interatomic forces in the domain of no interest. Thus, in this research, we determine the L-J parameters to replace the representative interactions between the gold nanoparticles and the substrate of mica through design sensitivity analysis and design optimization techniques. We also try to reduce the computing costs significantly by substituting the structure of substrate by a L-J potential wall. Due to the huge costs for the analysis of MD systems, a gradient-based approach and parallel computation are indispensable for the design optimization of nanoscale materials, which are so far not fully developed yet but essential for the future direction of nanoscale design optimization. There are two approaches in design optimization methods; a gradient-based design optimization [11] and a sampling-based one [19] which are not appropriate for the MD simulations due to the difference of governing equation and expensive computing costs. Therefore, we derive the design sensitivity for the MD simulations and perform a gradient-based design optimization for the best choice of potential parameters.

In the viewpoint of design aspects, temperature is one of the significant design variables that can be controlled to a value in simulations and experiments. The temperature effects of various properties of nanomaterials such as nanowires [20,21] and nanoparticles [22] were reported, using MD simulations. However, the method of studying temperature effects on nanomaterial properties relies on a trial and error approach. With the help of DSA, we can efficiently quantify the effects of parameters such as temperature on the results from MD simulations as well as experiments. Also, the gradient of simulation parameters can be changed when the operation temperature varies. Adjoint DSA method for the MD system where the number of atoms N, volume V and energy E is fixed (microcanonical (NVE) ensemble) was already proposed [17]. In this paper, we developed an adjoint DSA method for the constant temperature MD simulations. To obtain the continuous trajectory of a system having constant number N of atoms, volume V, and temperature T (canonical (NVT) ensemble), the Nosé–Hoover thermostat is utilized. The adjoint system of NVT ensemble is inherently path-dependent due to the additional degrees of freedom corresponding to the heat bath which acts as a damping term.

2. Design sensitivity analysis of extended MD systems

2.1. MD system with Nosé–Hoover thermostat

For MD simulations in a system where the number of particles N, volume V, and temperature T are fixed, a physical system is regarded as interacting with a heat bath. Hamiltonian for the extended system can be written, in terms of the extended variables [23,24], as

$$H\left(\tilde{p}, q, \tilde{p}_s, s\right) = \sum_{i=1}^{3N} \frac{\tilde{p}_i^2}{2m_i s^2} + \frac{\tilde{p}_s^2}{2Q} + V_{pot}(q) + z \ln s \tag{1}$$

where $\tilde{p}$, q, and V_{pot} are the momenta conjugate to q, atomic position, and potential energy function, respectively. $\tilde{p}$, S, and Q respectively denote the momentum conjugate to S, the additional degrees of freedom (DOFs) for the heat bath, and an effective mass associated with S. z is a factor for sampling canonical distribution. The upper tilde denotes the extended variables corresponding to the scaled time τ. The equations of motion for the extended system variables are described as

$$\frac{d\tilde{p}_i}{d\tau} \equiv -\frac{\partial H}{\partial q} = F_i \tag{2}$$

$$\frac{dq_i}{d\tau} \equiv \frac{\partial H}{\partial \tilde{p}_i} = \frac{\tilde{p}_i}{m_i s^2} \tag{3}$$

$$\frac{d\tilde{p}_s}{d\tau} \equiv -\frac{\partial H}{\partial s} = \sum_{i=1}^{3N} \frac{\tilde{p}_i^2}{m_i s^3} - z\frac{1}{s} \tag{4}$$

and

$$\frac{ds}{d\tau} \equiv \frac{\partial H}{\partial \tilde{p}_s} = \frac{\tilde{p}_s}{Q} \tag{5}$$

The relation between the physical time and the scale time τ in the extended system is given by

$$d\tau = sdt \tag{6}$$

If we sample the canonical distribution or calculate the ensemble average with the extended variable τ , the sampling is carried out at the integer multiples of the extended time step that are not constant. Therefore, for the sampling at equal intervals in physical time, it would be convenient to perform the integrations in terms of the physical system variables through the transformations and Eq. (6). Using the transformations, the equations of motion are written, in terms of the physical system variables and the heat bath variables, as

$$\dot{p}_i = F_i - p_i\frac{\dot{s}}{s} \tag{7}$$

$$\dot{q}_i = \frac{p_i}{m_i} \tag{8}$$

$$\dot{p}_s = \sum_{i=1}^{3N} \frac{p_i^2}{m_i} - z \tag{9}$$

and

$$\dot{s} = s\frac{p_s}{Q} \tag{10}$$

The second order Lagrangian equations of motion are written, in terms of physical variables which most often are used in the MD simulations by combining the first order equations of motion, as

$$\ddot{q}_i = \frac{F_i}{m_i} - \dot{q}_i\zeta \tag{11}$$

and

$$\dot{\zeta} = \frac{1}{Q}\left(\sum_{i=1}^{3N} m_i\dot{q}_i^2 - z\right) \tag{12}$$

where the friction coefficient $\zeta = \dot{s}/s$ is proposed by Hoover [25]. The factor z is determined, to recover a canonical sampling, by

$$z = 3Nk_BT \tag{13}$$

where N is the number of atoms in the physical system.

3. Adjoint variable method for extended MD systems

The finite difference method (FDM) and the direct differentiation method (DDM) are impractical to obtain the design sensitivity with respect to design variables due to huge amount of computational costs. Thus we employed the AVM which is efficient for the system of many design variables. The detailed adjoint DSA formulation for MD problems can be found in reference [26]. Compared to the NVE ensemble, the NVT ensemble has additional DOFs for thermostat variable in both the extended Hamiltonian and the equations of motion. A general performance measure ψ for the extended MD system can be defined, including both terminal value and time history quantity, as

$$\psi = g(\mathbf{b}, \zeta, \mathbf{q}, \dot{\mathbf{q}})|_{t=t_T} + \int_0^{t_T} h(\mathbf{b}, \zeta, \mathbf{q}, \dot{\mathbf{q}})dt \tag{14}$$

where $\mathbf{b}$ is a design variable vector. Taking the first order variation of Eq. (14) with respect to the design $\mathbf{b}$ and integrating by parts lead to

$$\begin{aligned}\psi' = &\left\{\frac{\partial g}{\partial \mathbf{b}}\delta\mathbf{b} + \frac{\partial g}{\partial \zeta}\zeta' + \left(\frac{\partial g}{\partial \mathbf{q}} + \frac{\partial h}{\partial \dot{\mathbf{q}}}\right)\mathbf{q}' + \frac{\partial g}{\partial \dot{\mathbf{q}}}\dot{\mathbf{q}}'\right\}_{t=t_T} \\ &+ \int_0^{t_T}\left\{\frac{\partial h}{\partial \mathbf{b}}\delta\mathbf{b} + \frac{\partial h}{\partial \zeta}\zeta' + \left(\frac{\partial h}{\partial \mathbf{q}} - \frac{d}{dt}\frac{\partial h}{\partial \dot{\mathbf{q}}}\right)\mathbf{q}'\right\}dt\end{aligned} \tag{15}$$

where $(\cdot)' = (d(\cdot)/d\mathbf{b})\,\delta\mathbf{b}$ and as being independent of design, the initial conditions for the design sensitivity are selected as $\mathbf{q}'(0) = \dot{\mathbf{q}}'(0) = \mathbf{0}$. To efficiently evaluate Eq. (15), the implicit dependence terms are removed by using the adjoint system responses. Using the Nosé–Hoover thermostat [23–25], the equations of motion of Eqs. (11) and (12) can be rewritten, in matrix–vector forms, as

$$\mathbf{m}_A\ddot{\mathbf{q}}(t) = \mathbf{f} - \zeta(t)\mathbf{m}_A\dot{\mathbf{q}}(t) \tag{16}$$

where the thermostat variable is obtained by solving the following equation,

$$Q\dot{\zeta}(t) = \dot{\mathbf{q}}(t)^T\mathbf{m}_A\dot{\mathbf{q}}(t) - z \tag{17}$$

where Q denotes the effective masses associated with the thermostat variable $\zeta(t)$. For sampling canonical distribution, a factor is introduced as $z = 3Nk_BT$, where N, k_B, and T denote the number of atoms, Boltzmann constant, and desired temperature in the ensemble, respectively. Note that coupling between the ensembles is found through q in the inter-atomic force term in Eqs. (16) and (17). Introducing two adjoint variables $\lambda(t)$ and $\xi(t)$ that are assumed to be independent of the design, the following should hold for all the time span.

$$\begin{aligned}&\int_0^{t_T} \lambda^T\left\{\mathbf{m}_A(\mathbf{b})\ddot{\mathbf{q}} - \mathbf{f}(\mathbf{b}, \mathbf{q}) + \mathbf{m}_A(\mathbf{b})\zeta\dot{\mathbf{q}}\right\}dt \\ &\quad + \int_0^{t_T} \xi\left\{Q(\mathbf{b})\dot{\zeta} - \dot{\mathbf{q}}^T\mathbf{m}_A(\mathbf{b})\dot{\mathbf{q}} + z(\mathbf{b})\right\}dt = 0\end{aligned} \tag{18}$$

Taking the first order variation of Eq. (18) and integrating by parts yield

$$\begin{aligned}&\left\{\lambda^T\mathbf{m}_A\dot{\mathbf{q}}' + \left(\lambda^T\zeta\mathbf{m}_A - \dot{\lambda}^T\mathbf{m}_A - 2\xi\dot{\mathbf{q}}^T\mathbf{m}_A\right)\mathbf{q}' + \xi Q\zeta'\right\}_{t=t_T}\\ &\quad + \int_0^{t_T}\left(\ddot{\lambda}^T\mathbf{m}_A - \lambda^T\frac{\partial\mathbf{f}}{\partial\mathbf{q}} - \dot{\lambda}^T\zeta\mathbf{m}_A\right.\\ &\quad \left. -\lambda^T\dot{\zeta}\mathbf{m}_A + 2\xi\ddot{\mathbf{q}}^T\mathbf{m}_A + 2\dot{\xi}\dot{\mathbf{q}}^T\mathbf{m}_A\right)\mathbf{q}'dt\\ &\quad + \int_0^{t_T}\left(\lambda^T\mathbf{m}_A\dot{\mathbf{q}} - \dot{\xi}Q\right)\zeta'dt\\ &= -\int_0^{t_T}\left\{\lambda^T\left(\frac{\partial\mathbf{m}_A}{\partial\mathbf{b}}\ddot{\mathbf{q}} - \frac{\partial\mathbf{f}}{\partial\mathbf{b}} + \frac{\partial\mathbf{m}_A}{\partial\mathbf{b}}\zeta\dot{\mathbf{q}}\right)\right.\\ &\quad \left. +\xi\left(\frac{\partial z}{\partial\mathbf{b}} + \frac{\partial Q}{\partial\mathbf{b}}\dot{\zeta} - \dot{\mathbf{q}}^T\frac{\partial\mathbf{m}_A}{\partial\mathbf{b}}\dot{\mathbf{q}}\right)\right\}\delta\mathbf{b}dt\end{aligned} \tag{19}$$

Comparing the resulting identity of Eq. (19) with Eq. (15), the following adjoint systems are obtained together with the corresponding terminal conditions for the MD systems of NVT ensemble.

$$\ddot{\lambda} = \zeta\dot{\lambda} + \mathbf{m}_A^{-1}\frac{\partial\mathbf{f}}{\partial\mathbf{q}}\lambda + \dot{\zeta}\lambda - 2\xi\ddot{\mathbf{q}} - 2\dot{\xi}\dot{\mathbf{q}} + \mathbf{m}_A^{-1}\left(\frac{\partial h}{\partial\mathbf{q}} - \frac{d}{dt}\frac{\partial h}{\partial\dot{\mathbf{q}}}\right)^T \tag{20}$$

$$\dot{\xi} = \frac{1}{Q}\left(\lambda^T\mathbf{m}_A\dot{\mathbf{q}} - \frac{\partial h}{\partial\zeta}\right) \tag{21}$$

$$\xi(t_T) = \frac{1}{Q}\frac{\partial g}{\partial\zeta} \tag{22}$$

$$\lambda(t_T) = \mathbf{m}_A^{-1}\left(\frac{\partial g}{\partial\dot{\mathbf{q}}}\right)^T \tag{23}$$

and using Eqs. (22) and Eqs. (23),

$$\dot{\lambda}(t_T) = \mathbf{m}_A^{-1}\left\{\zeta\left(\frac{\partial g}{\partial\dot{\mathbf{q}}}\right)^T - \left(\frac{\partial g}{\partial\mathbf{q}} + \frac{\partial h}{\partial\dot{\mathbf{q}}}\right)^T\right\} - \frac{2}{Q}\left(\frac{\partial g}{\partial\zeta}\right)\dot{\mathbf{q}}. \tag{24}$$

Thus, the adjoint design sensitivity can be obtained as

$$\begin{aligned}\psi' = &\left.\frac{\partial g}{\partial\mathbf{b}}\delta\mathbf{b}\right|_{t=t_T} + \int_0^{t_T}\left\{\frac{\partial h}{\partial\mathbf{b}} - \lambda^T\left(\frac{\partial\mathbf{m}_A}{\partial\mathbf{b}}\left(\ddot{\mathbf{q}} + \zeta\dot{\mathbf{q}}\right) - \frac{\partial\mathbf{f}}{\partial\mathbf{b}}\right)\right.\\ &\left. -\xi\left(\frac{\partial z}{\partial\mathbf{b}} + \frac{\partial Q}{\partial\mathbf{b}}\dot{\zeta} - \dot{\mathbf{q}}^T\frac{\partial\mathbf{m}_A}{\partial\mathbf{b}}\dot{\mathbf{q}}\right)\right\}\delta\mathbf{b}dt\end{aligned} \tag{25}$$

Note that Eq. (25) requires the original and the adjoint responses. For detailed derivation and discussions, interested readers may refer to Jang and Cho [26].

4. Reduced model for silicate substrate

To precisely mimic the nanoscale behaviors observed from experiments, the accurate modeling and determination of interatomic potential parameters are crucial for the successful MD simulations. A sufficient number of layers is necessary to consider the bulk characteristics of substrates, especially when substrates are involved. Despite the efforts to reduce the size of substrates, e.g. utilizing periodic boundary conditions and freezing several bottom layers, the structure of substrates requires special treatments in interatomic force terms such as bonding, angle, dihedral, and improper ones in most cases. These special treatments generally lead to the tremendous increase of computational costs even for simple metallic nanostructures. Furthermore, only limited sort of substrate structures and the force field parameters are available due to the empirical nature of fitting parameters matching the bulk properties of target materials. It is well known that these drawbacks make it difficult to fulfill the needs of rapidly increasing interest of correlating the MD simulations to the physical experiments.

Consider the cold welding problem of gold nanoparticles on a silicate substrate[27–29] in Fig. 1. Despite not the main subject of MD simulations, the silicate substrate consumes most of the computational costs. Therefore, we replace the complicated and time-consuming silicate structure with a multiple layer model of 12–6 L-J potential wall, through a gradient-based design optimization whose design variables include ϵ, σ, and the positions of each layer. When the substrates and the nanostructures consist of different materials, the interactions between them are generally represented by Lennard-Jones type interactions regardless of interatomic potentials utilized in each material. With the proper parameters and positions of multiply layered L-J potential walls determined from the design optimization, we successfully reproduce the behavior of the silicate substrate while dramatic saving is achieved in computational costs.

4.1. Modeling details

We construct two numerical models; a full model of gold nanoparticles on the mica substrate as a reference for the optimization and a reduced model of gold nanoparticles on the potential walls. The full model is analyzed by the established MD simulation package LAMMPS to make the reference for the optimization[30]. The gold nanoparticles are thermally equilibrated independently at 300 K for 1 ns. The time step of 1 fs is used together with a Nosé–Hoover thermostat. We used the EAM (Embedded Atom Method) interatomic potential for gold atoms [31,32]. After the thermal equilibration of gold nanoparticles, they are placed on the mica substrate consisting of 2688 atoms of 5 types, 3840 bonds of 3 harmonic bond types, and 9,984 angles of 6 harmonic angle types. Then, additional thermal equilibration is performed for 10 ps at 300 K with the time step of 1 fs using the Nosé–Hoover thermostat. Finally, the kinematic information of gold nanoparticles is transferred to the reduced one to impose the same initial conditions. The detailed information of pairwise, bond, and angle force field parameters are shown in Tables 1–3. The pairwise terms for different atom types are obtained from the Lorentz–Berthelot mixing rule. The Lennard-Jones parameters for gold atoms are referred from Merabia et al. [33].

4.2. Formulation of design optimization problem

Consider the gold nanoparticles placed on a mica substrate as shown in Fig. 1(a). The objective is to determine the position and the proper Lennard-Jones force field parameters (energy depth ϵ and collision diameter σ of subdomain in each layer of multi-layered potential wall as shown in Fig. 1(b), through gradient-based design optimization. The initial positions of L-J potential walls are obtained from the z-directional center of mass of each atomic layer of the mica substrate. Due to the cut off radius in the MD simulations, the first 11 atomic layers of mica substrate are selected. Therefore, the total number of design variables is 22 and their initial values are chosen as the L-J parameters utilized for interactions between the gold and the atoms consisting of the mica. A design optimization problem is formulated, as shown in Fig. 2, as

Minimize

$$\psi = \frac{\int_0^{t_T} w(t)\left\{\Phi^m_{reduced}(t) - \Phi^m_{full}(t)\right\}^2 dt}{\int_0^{t_T} w(t)dt} \tag{26}$$

Subjected to

$$\begin{aligned}&0.0001 \le \varepsilon_i \le 100 \quad (i = 1, \ldots, ndv1)\\ &0.1 \le \sigma_j \le 100 \quad (j = 1, \ldots, ndv2)\\ &\mathbf{x}_l \le \mathbf{x}_k \le \mathbf{x}_u \quad (k = 1, \ldots, ndv3)\end{aligned} \tag{27}$$

The objective is to minimize the squared difference of time averaged performance of gold nanoparticles between the full and the reduced models during the whole time span. It is an unconstrained optimization problem only with the side constraints for the design variables ε_i, σ_j, and $\mathbf{x}_k$ as shown in Eq. (27). A gradient-based

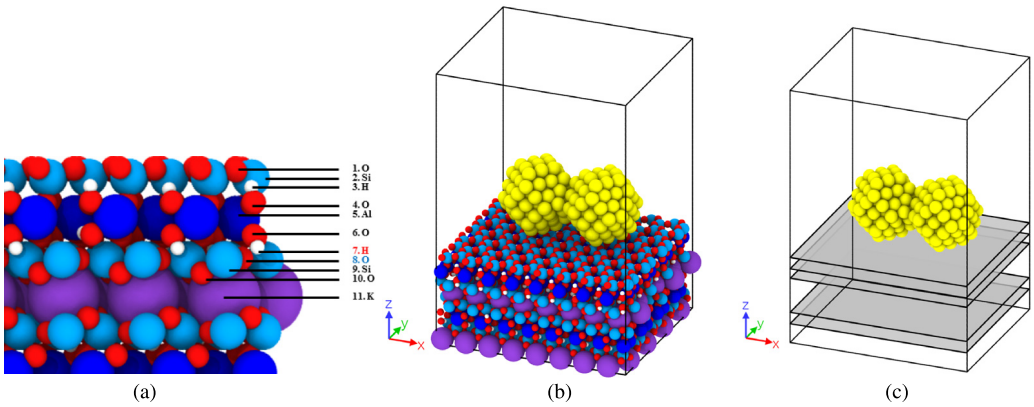

Fig. 1. Reduced (multiple layer L-J potential wall) model for silicate substrate. (a) Modeling of mica substrate (b) Full (mica substrate) model (c) Reduced model.

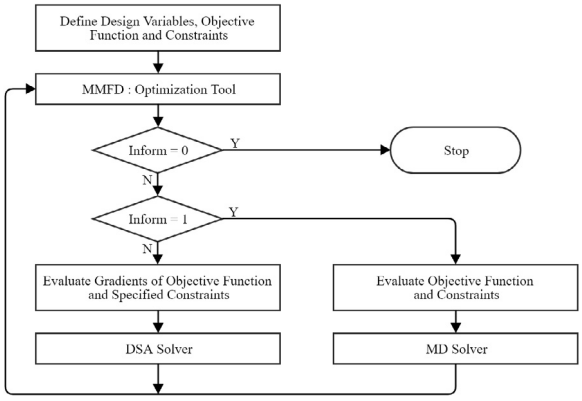

Fig. 2. Scheme for automated design optimization.

optimization algorithm for unconstrained optimization method, Broyden–Fletcher–Goldfarb–Shanno (BFGS), is utilized to solve the aforementioned optimization problem, where the required gradient values are provided by the developed adjoint DSA method [17]. The algorithm for the automated design optimization procedure [34] is illustrated in Fig. 2. The design variables (ε_i , σ_j, and $\mathbf{x}_k$) and objective function (ψ) are supplied to the optimization tool BFGS. If the control parameter "*inform*" is equal to zero, the optimization is completed. If *inform*=1, the objective function and constraints are evaluated. If *inform*=2, the gradients of those are evaluated.

5. Results and discussions

5.1. Verification of reduced model: Cold welding of gold nanoparticles [31]

In Fig. 3, the performance of reduced models (In-house, LAMMPS [30]) is compared with that of the full model (Mica). The reduced models employ the potential walls instead of mica substrate. The L-J parameters for interactions between gold and each atom in the mica substrate are utilized for the reduced models, which match very well as shown in Fig. 3. MD simulations with NVT ensemble are performed for 20 ps using the time step of 0.1 fs. The reduced models show similar potential energy trajectory at early time of simulation, compared to the full model (Mica). However, the trajectory starts to deviate after 2.5 ps and the difference becomes significant after 20 ps.

Comparing the configurations of full model (Mica) at initial and terminal time steps in Fig. 4(a), the initial nanoparticles (yellow) are agglomerated and shrunk at terminal time (green). The clearance between the nanoparticles and the mica substrate is maintained during the whole time span. However, comparing the configurations of full (yellow) and reduced (red) models at terminal time in Fig. 4(b), the nanoparticles in the reduced model are floating above the mica substrate surface. This indicates that the attraction force between the multi-layer potential walls and the nanoparticle is insufficient compared with the full model. Thus, it is necessary to determine appropriate L-J parameters to make the performance of the reduced model as close as that of the full model.

Table 1
Pairwise force field parameters.

Atom type	ϵ (eV)	σ (Å)
Al	0.0021682	3.74178
H	0.0005637	0.97830
K	0.0086729	3.38542
O	0.0010841	3.11815
Si	0.0021682	3.56359

5.2. Optimal potential parameters for multiple layers

In this section, the optimal potential parameters are determined using a gradient based optimization algorithm. The total number of design variables is 22 (energy depth and collision diameter of each or the 11 layers of L-J potential wall). Since the MD simulation is used to solve a transient dynamic problem, it is not always possible to improve the performances in whole time span. However, we can improve the performance measure selectively at some time steps. In Fig. 3, we can notice that the reduced models start to deviate from the full model at the time step of 23,400 and maintain the difference after that. In this optimization problem, the objective is to minimize the squared difference of time averaged potential energy between 23,400 and 36,200 time steps.

Minimize

$$\psi = \frac{1}{t_2 - t_1} \int_{t_1}^{t_2} w(t) \left\{ \Phi^m_{reduced}(t) - \Phi^m_{full}(t) \right\}^2 dt,$$
$$t_1 = 23,400,\ t_2 = 36,200 \tag{28}$$

Subjected to

$$\begin{aligned} 0.0001 \le \varepsilon_i \le 100 \quad (i = 1, \ldots, 11) \\ 0.1 \le \sigma_j \le 100 \quad (j = 1, \ldots, 11) \end{aligned} \tag{29}$$

Fig. 4 shows the history of potential energy of gold nanoparticles (AuNPs) in the reduced and the full models after the optimization of potential parameters. The difference of potential energies between the reduced and the full models is significantly reduced

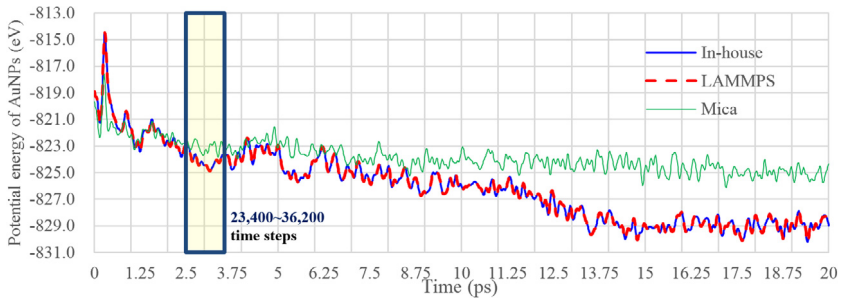

Fig. 3. Potential energy in reduced (Mica, In-house) and full (LAMMPS) models.

Table 2
Harmonic bond distance.

Bond type	K (eV/Å^2)	Equilibrium bond distance (Å)
Al-O	37.2935	1.940
H-O	42.9309	0.929
Si-O	37.2935	1.640

Table 3
Harmonic angle.

Angle type	K (eV/rad^2)	Equilibrium angle (°)
Al-O-Al	14.7440	109.5
Al-O-H	0.9974	116.2
Al-O-Si	14.7440	109.5
O-Al-O	14.7440	95.0
O-Si-O	14.7440	109.5
Si-O-Si	14.7440	109.5

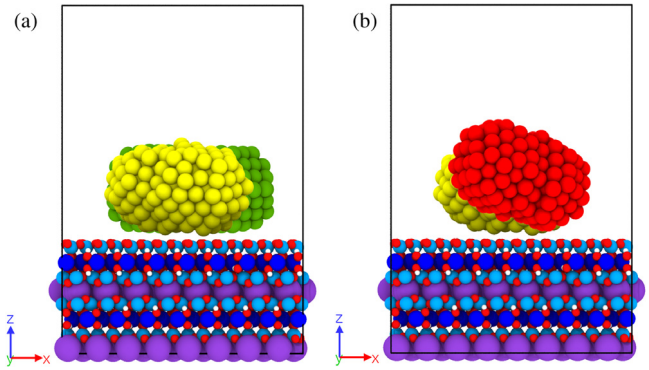

Fig. 4. Configuration comparison at terminal time. (a) Full model (Mica) (b) Full (yellow) and reduced (red) models. (For interpretation of the references to color in this figure legend, the reader is referred to the web version of this article.)

around the terminal time, which is due to the optimal determination of potential parameters by reducing the deviation tendency between 23,400 and 36,200 time steps (see Fig. 5).

Comparing the configurations of full model (Mica) at initial and terminal time steps in Fig. 6(a), the initial nanoparticles (green) are agglomerated and shrunk at terminal time (yellow). Fig. 6(b) shows the configuration of the full (yellow) and the reduced optimal (red) models at terminal time. In the reduced optimal (red) model, the clearance between the nanoparticles and the mica substrate is maintained during the whole time span. This indicates that the attraction force between the multi-layer potential walls and the nanoparticle is optimally determined compared with the full model.

The optimization process is quite convergent; the MD simulations are performed 39 times and gradients are evaluated 6 times. The objective function of Eq. (28) is monotonically decreased as shown in Fig. 7.

Optimally determined design variables are compared with the original values in Table 4. Generally, the variables (energy depth ϵ and collision diameter σ) at all the layers increase except for the first layer. Comparing the computational costs for one MD simulation using LAMMPS in Table 5, the reduced model requires only 1.77

5.3. Optimal potential parameters for sub-divided single layer

Consider a reduced model with the sub-divided single layer of L-J potential wall in Fig. 8, where the image of mica is inserted in Fig. 8(b) just for the visualization purpose of sub-divided single layer. The single layer is divided into 16 segments and the dimension of each segment is 10.3836 × 9.0154. The single potential wall is used instead of the mica substrate in Fig. 8(a). Three models are constructed to verify the effectiveness of potential wall of sub-divided single layer; (A) sub-divided potential wall model (in-house), (B) single layer potential wall model (in-house), and (C) single layer potential wall model (LAMMPS). Initial potential parameters for all the models are $\varepsilon = 0.0061149$, $\sigma = 3.6000$, which stand for the characteristics of hydrogen atoms.

In Fig. 9, the performance of sub-divided potential wall models (A) is compared with that of the single potential wall models (B, C). MD simulations with NVT ensemble are performed for 50 ps using

Table 4
Comparison of design variables.

Layer	ϵ			σ		
	(a) Original	(b) Optimal	(b)/(a) (%)	(c) Original	(d) Optimal	(d)/(c) (%)
1	6.1149e−03	5.5216e−04	9.0298	3.6000	3.3921	94.2263
2	1.9149e−03	1.3794e−01	7203.6054	3.2488	3.2520	100.0978
3	9.7640e−04	4.3133e−03	441.7581	1.9562	1.9562	100.0019
4	6.1149e−03	4.6868e−02	766.4584	3.6000	3.6050	100.1383
5	1.9149e−03	1.1970e−02	625.1031	3.3379	3.3383	100.0113
6	6.1149e−03	1.0833e−02	177.1568	3.6000	3.6006	100.0171
7	9.7640e−04	1.0369e−03	106.1984	1.9562	1.9562	100.0000
8	6.1149e−03	7.3242e−03	119.7769	3.6000	3.6002	100.0044
9	1.9149e−03	2.4369e−03	127.2601	3.2488	3.2488	100.0006
10	6.1149e−03	6.1203e−03	100.0883	3.6000	3.6000	100.0000
11	3.8298e−03	3.8298e−03	100.0000	3.1597	3.1597	100.0000

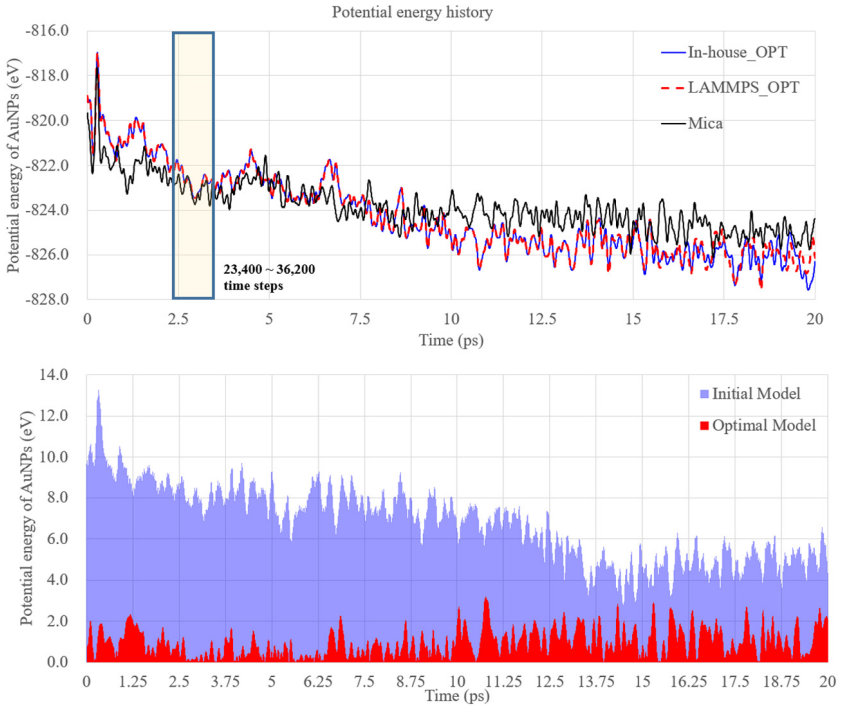

Fig. 5. Multi-layer potential wall (In-house OPT, LAMMPS OPT) and full model (Mica) (top: a comparison of the full mica model and OPT model, bottom: purple section indicates potential energy difference between potential wall model with initial parameters and full mica model, red section indicates potential energy difference between potential wall model with optimized parameters and full mica model). (For interpretation of the references to color in this figure legend, the reader is referred to the web version of this article.)

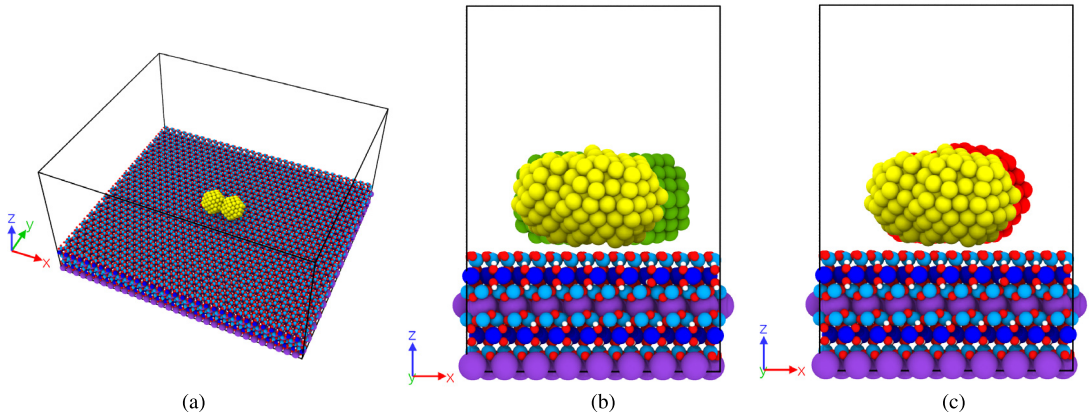

Fig. 6. Configuration comparison at terminal time: (a) Full model (Mica), (b) Full (yellow) and reduced optimal (red). (For interpretation of the references to color in this figure legend, the reader is referred to the web version of this article.)

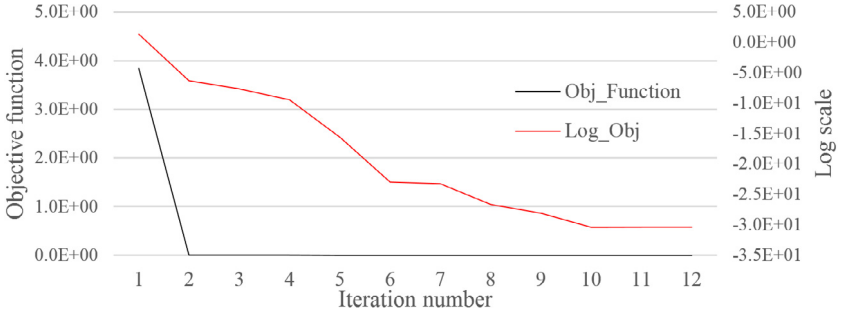

Fig. 7. Optimization history (6 gradient calls, 39 function calls).

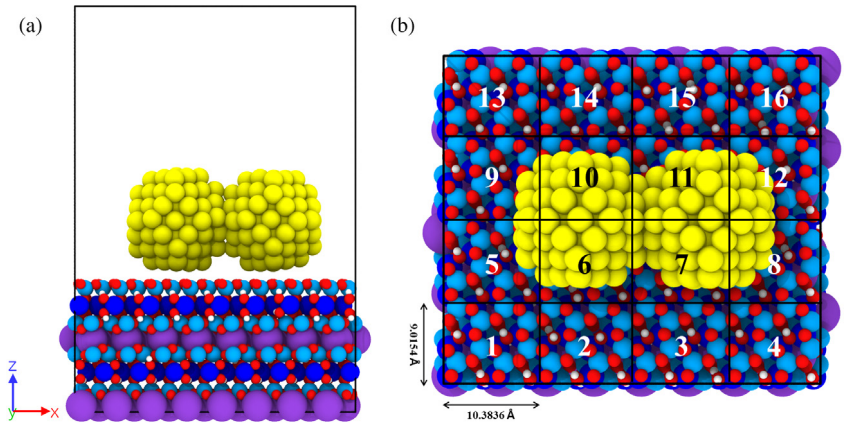

Fig. 8. Mica and gold nanoparticle models (a) Full model (front view) (b) Sub-divided single layer model (top view).

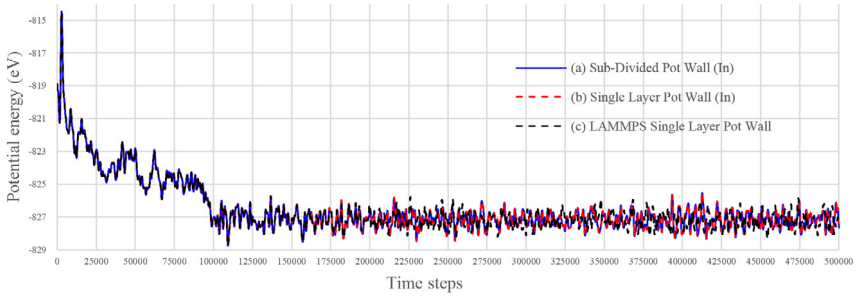

Fig. 9. Comparison of various potential wall models.

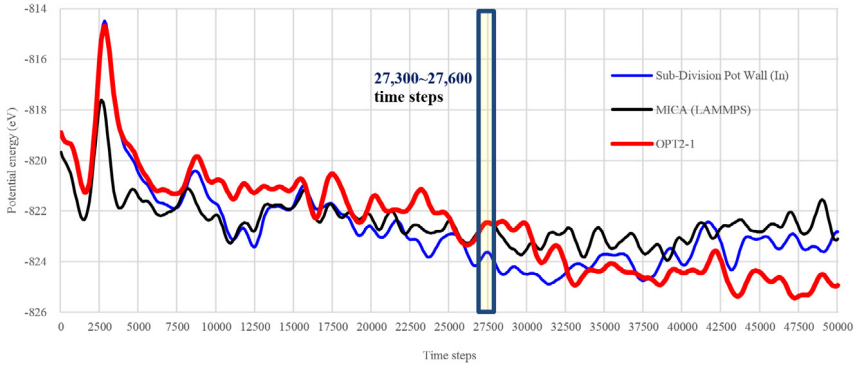

Fig. 10. Potential energy in model A (blue), model C (black), and optimal model A (red). (For interpretation of the references to color in this figure legend, the reader is referred to the web version of this article.)

Table 5
Comparison of computation costs (LAMMPS).

(a) Full model (sec)	(b) Reduced model (sec)	(b)/(a) (%)
4739.48	84.0308	1.7730

the time step of 0.1 fs. Model (A) shows similar potential energy trajectory compared to the other models (B, C).

Using the gradient based optimization algorithm, we determine the optimal L-J potential parameters for sub-divided single layer model (A). The total number of design variables is 32 (energy depth ϵ and collision diameter σ in each segment of L-J potential wall). In this optimization problem, the objective is to minimize the squared difference of time averaged potential energy of mica and sub-divided single layer potential wall model between 27,300 and 27,600 time steps. The objective is to minimize the time averaged potential energy between 27,300 and 27,600 steps.

Minimize

$$\psi = \frac{1}{t_2 - t_1} \int_{t_1}^{t_2} w(t) \left\{ \Phi_A^m(t) - \Phi_C^m(t) \right\}^2 dt,$$

$$t_1 = 27,300, t_2 = 27,600, \tag{30}$$

Subjected to

$$\begin{aligned} 0.0001 \le \varepsilon_i \le 100 \quad (i = 1, \ldots, 16) \\ 0.1 \le \sigma_j \le 100 \quad (j = 1, \ldots, 16) \end{aligned} . \tag{31}$$

Fig. 10 compares the history of potential energy in models A and C, and the optimal model of A, up to 50,000 time steps. The potential energies in models A (blue) and C (black) show similar tendency until around 26,000 time steps but its difference starts

Table 6
Optimization results.

Segment	ϵ			σ		
	(a) Original	(b) Optimal	(b)/(a) (%)	(c) Original	(d) Optimal	(d)/(c) (%)
1	6.1149e−03	6.1149e−03	100.0000	3.6000	3.6000	100.0000
2		6.1149e−03	100.0000		3.6000	100.0000
3		6.1149e−03	100.0000		3.6000	100.0000
4		6.1149e−03	100.0000		3.6000	100.0000
5		5.3916e−03	88.1674		3.5998	99.9940
6		1.4557e−03	23.8063		3.5977	99.9370
7		1.6910e−02	276.5442		3.6046	100.1285
8		6.5386e−03	106.9283		3.6002	100.0067
9		5.8116e−03	95.0395		3.5999	99.9972
10		8.0306e−04	13.1328		3.5977	99.9364
11		1.6961e−02	277.3777		3.6055	100.1537
12		6.0390e−03	98.7588		3.6000	100.0004
13		6.1149e−03	100.0000		3.6000	100.0000
14		6.1149e−03	100.0000		3.6000	100.0000
15		6.1149e−03	100.0000		3.6000	100.0000
16		6.1149e−03	100.0000		3.6000	100.0000

to increase between 27,300 and 27,600 time steps. Notice that the potential energy in the optimal model A (red) still has some deviation from model C (black) but matches very well between 27,300 and 27,600 time steps. The optimization process is quite convergent and the objective function of Eq. (30) is monotonically decreased.

Optimally determined design variables are compared with the original values in Table 6. Notice that there are some changes in the variables (energy depth ϵ and collision diameter σ) of the segments around the nanoparticles and the energy depth especially varies significantly.

6. Conclusions

Only limited sort of substrate structures and the force field parameters are available due to the empirical nature of fitting parameters matching the bulk properties of target materials. It is well known that these drawbacks make it difficult to fulfill the needs of rapidly increasing interest of correlating the MD simulations to the physical experiments. Thus, we developed an adjoint DSA method for the constant temperature MD simulations with a Nosé–Hoover thermostat. In numerical examples, with the proper parameters and positions of multiple layer L-J potential walls determined by design optimization, we successfully reproduce the behavior of silicate substrate while dramatically saving is achieved in computational costs. The difference of potential energies between the reduced and the full models is significantly reduced around the terminal time, which is due to the optimal determination of potential parameters by reducing the deviation tendency during some time steps. Comparing the computational costs for one MD simulation using LAMMPS, the reduced model requires only 1.77.

Acknowledgment

This work was supported by the National Research Foundation of Korea (NRF) grant funded by the Korea government (MSIP) (No. 2010-0018282).

References

[1] D.A. Brant, P.J. Flory, J. Am. Chem. Soc. 87 (1965) 2791–2800.
[2] R.A. Scott, H.A. Scheraga, J. Chem. Phys. 42 (1965) 2209–2215.
[3] J.C. Slater, J.G. Kirkwood, Phys. Rev. 37 (1931) 682–697.
[4] A. Bondi, J. Phys. Chem. 68 (1964) 441–451.
[5] J.O. Hirschfelder, Adv. Chem. Phys. 12 (1967) 329.
[6] S.J. Marrink, H.J. Risselada, S. Yefimov, D.P. Tieleman, H.A. de Vries, J. Phys. Chem. B 111 (2007) 7812–7824.
[7] A.P. Lyubartsev, A. Laaksonen, Phys. Rev. E 52 (1995) 3730.
[8] D. Reith, M. Putz, F. Muller-Plathe, J. Comput. Chem. 24 (2003) 1624–1636.
[9] S. Izvekov, A.G. Voth, J. Chem. Phys. 123 (2005) 134105.
[10] E.J. Haug, K.K. Choi, V. Komkov, Design Sensitivity Analysis of Structural Systems, Academic Press, New York, 1986.
[11] S. Cho, K.K. Choi, Internat. J. Numer. Methods Engrg. 48 (2000) 351–373.
[12] S. Cho, K.K. Choi, Internat. J. Numer. Methods Engrg. 48 (2000) 375–399.
[13] C.C. Hsieh, J.S. Arora, Comput. Methods Appl. Mech. Engrg. 43 (1984) 195–219.
[14] J.J. Tsay, J.S. Arora, Comput. Methods Appl. Mech. Engrg. 81 (1990) 183–208.
[15] M.-G. Kim, H.-L. Jang, S. Cho, J. Comput. Phys. 240 (2013) 1–19.
[16] M.-G. Kim, H.-L. Jang, H.-S. Kim, S. Cho, Model. Simul. Mater. Sci. Eng. 21 (3) (2013) 035005.
[17] H.-L. Jang, J.-H. Kim, Y. Park, S. Cho, Int. J. Mech. Mater. Des. 10 (2014) 379–394.
[18] M.I. Mendelev, S. Han, D.J. Srolovitz, Philo. Mag. 83 (35) (2003) 3977–3994.
[19] J.S. Arora, Introduction to Optimum Design, Elsevier, Taiwan, 2016.
[20] S.J.A. Koh, H.P. Lee, Nanotechnology 17 (14) (2006) 3451–3467.
[21] H.A. Wu, Mech. Res. Commun. 33 (2006) 9–16.
[22] Y. Shibuta, T. Suzuki, J. Chem. Phys. 129 (14) (2008) 144102.
[23] S. Nosé, Mol. Phys. 52 (1984) 255–268.
[24] S. Nosé, J. Chem. Phys. 81 (1984) 511–519.
[25] W.G. Hoover, Phys. Rev. A 31 (1985) 1695–1697.
[26] H.-L. Jang, S. Cho, Int. J. Mech. Mater. Des. 13 (2) (2017) 243–252.
[27] S.-H. Cha, Y. Park, J.W. Han, K. Kim, H.-S. Kim, H.-L. Jang, S. Cho, Sci. Rep. (2016) srep32951.
[28] Y. Choi, M.-J. Choi, S.-H. Cha, Y.S. Kim, S. Cho, Y. Park, Nanoscale Res. Lett. 9 (103) (2013).
[29] H.J. Noh, A.R. Im, H. -S. Kim, J.K. Sohng, C.K. Kim, Y.S. Kim, S. Cho, Y. Park, J. Nanosci. Nanotechnol. 12 (5) (2012) 3884–3895.
[30] S. Plimpton, J. Comput. Phys. 1117 (1995) 1–19.
[31] S.M. Foiles, M.I. Baskes, M.S. Daw, Phys. Rev. B. 33 (12) (1986) 7983–7991.
[32] M.S. Daw, S.M. Foiles, M.I. Baskes, Mater. Sci. Rep. 9 (7–8) (1993) 251–310.
[33] S. Merabia, S. Shenogin, L. Joy, P. Keblinski, J. -L. Barrat, Proc. Natl. Acad. Sci. USA 106 (36) (2009) 15113–15118.
[34] G.N. Vanderplaats, Numerical Optimization Techniques for Engineering Design, third ed., VR & D, 1999.